

UC Santa Cruz

UC Santa Cruz Previously Published Works

Title

Ferrovolcanism: Iron Volcanism on Metallic Asteroids

Permalink

<https://escholarship.org/uc/item/6tr2t68k>

Journal

Geophysical Research Letters, 46(10)

ISSN

0094-8276

Authors

Abrahams, Jacob NH
Nimmo, Francis

Publication Date

2019-05-28

DOI

10.1029/2019gl082542

Peer reviewed



Published in final edited form as:

Geophys Res Lett. 2019 May 28; 46(10): 5055–5064. doi:10.1029/2019gl082542.

Ferrovolcanism: Iron Volcanism on Metallic Asteroids

Jacob N. H. Abrahams¹, Francis Nimmo¹

¹Department of Earth and Planetary Science, University of California Santa Cruz, Santa Cruz, CA 95064

Abstract

Metallic asteroids, the exposed cores of disrupted planetesimals, are expected to have been exposed while still molten. Some would have cooled from the outside in, crystallizing a surface crust which would then grow inward. Because the growing crust is expected to be more dense than the underlying melt, this melt will tend to migrate toward the surface whenever it is able. Compressional stresses produced in the crust while it cools will be relieved locally by thrust faulting, which will also provide potential conduits for melt to reach the surface. We predict iron volcanism to have occurred on metallic asteroids as they cooled and discuss the implications of this process for both the evolution and the modern appearance of these bodies.

1 Introduction

Three major types of crustal material are observed in the solar system. The most familiar, silicate crust, is found on the terrestrial planets and their moons, most asteroids, and on Io. The other common type of crust is formed from ices, primarily water ice, on the surfaces of most outer solar system moons, some asteroids, and most Kuiper belt objects. In addition to ice and silicates, a less common third type of crust is present in the solar system: metallic core material left behind following collisional disruption of the mantle of a differentiated body (Asphaug et al., 2006; Yang et al., 2007). These bodies have been detected in the asteroid belt (Matter et al., 2013; Neeley et al., 2014) and contribute substantially to the meteorite record (Hutchison, 2004). However, our understanding of their surfaces is very limited – the first detailed images of a metallic asteroid will come from the Psyche spacecraft, which is scheduled to launch in 2022 (Lord et al., 2017).

Volcanism occurs throughout the solar system in a variety of different forms (e.g. Lopes & Gregg, 2004; Wilson, 2009). All terrestrial planets (and Io) exhibit silicate volcanism, and a number of icy bodies display either geomorphic signs of cryovolcanism (Moore et al., 2016; Schenk et al., 2001) or directly observed plume behavior (Porco et al., 2006; Roth et al., 2014). In this paper we explore the question of whether metallic bodies can host their own novel style of volcanism. Metallic volcanism should bear most resemblance to silicate volcanism, where the melt is buoyant relative to the solid matrix. This is in contrast to cryovolcanism, where the melt is more dense and mechanisms other than buoyancy are needed to aid its ascent (e.g. Crawford & Stevenson, 1988; Manga & Wang, 2007). The

main differences between iron volcanism and silicate volcanism are the lower viscosity of liquid metal, the higher ductility of solid metal, metal's higher resistance to fracture and the likely absence of a low-density metallic crust able to stall fluid migration. In addition, our analysis is concerned with a body hosting an iron 'magma ocean', where the entire interior is molten, rather than broad regions of low melt fraction or magma confined to small chambers.

All but the smallest differentiated bodies will have partially molten iron cores for at least the first ~100 million years of the solar system, the period in which their mantles are most likely to be removed (Bottke et al., 2005). When a fully molten core is then exposed to space, it will rapidly form a quench crust on the surface. This new crust will either sink, exposing new melt to space and rapidly freezing the whole body, or it will be supported by its own strength and crystallize slowly from the outside in. Crucially, observations of cooling rate-Ni correlations indicate that some asteroid bodies crystallize from the outside-in (Chabot & Haack, 2006; Yang et al., 2007, 2008), which is the mode of solidification of interest to this work. These observations show that, within the IVA meteorite family, the samples with the fastest cooling rates have the lowest incompatible element contents, implying that the shallowest material crystallizes first i.e. top-down solidification. While this explanation is not universally accepted (Albarède et al., 2013), for the purpose of this paper we assume it is correct; further aspects of solidification are addressed in Scheinberg et al. (2016) and Neufeld et al. (2019). We predict that in such bodies the buoyant melt beneath the crust will periodically be able to erupt, influencing their cooling and creating volcanic features on the surface.

The aim of this manuscript is to investigate the basics of metallic volcanism. Because iron volcanism is a novel concept, and many of the important parameters are poorly constrained, we take an order-of-magnitude approach whenever possible and are only seeking to make approximate predictions for the real behavior. First we discuss the thermal and mechanical evolution of an initially molten metallic asteroid. Then we address the ability of melt to reach the surface and challenges to that migration. We conclude by discussing some features of how metallic volcanism may present itself, and the need for continuing work anticipating its morphology, looking for it in current records, and collecting additional data.

2 Thermal Evolution

2.1 Thermal evolution prior to disruption

Bodies formed in the first ~2.5 Myr of the solar system will possess enough short lived radionuclides, particularly ^{26}Al , to melt and separate metals and silicates (Goldstein et al., 2009; Hevey & Sanders, 2006). In the absence of mantle convection (Tkalcic et al., 2013) or silicate melt advection, the core will not begin to cool significantly until a conductive cooling wave has propagated to the base of the mantle. For a thermal diffusivity of $\approx 10^{-6} \text{ m}^2/\text{s}$ (Carslaw & Jaeger, 1959), even a 60 km mantle has a thermal timescale of 100 Myr. Since 16 Psyche, the largest metallic asteroid, has an average radius over 100 km (Shepherd et al., 2017) its mantle thermal timescale prior to disruption will have exceeded this value. Because disruption most likely occurred during terrestrial planet accretion (Bottke et al.,

2005), the cores of proto-Psyche and other similar-sized asteroids will have been molten when disruption occurred.

2.2 Thermal evolution after disruption

After disruption (and any requisite reaccretion, which will be rapid - on orbital timescales) the body of interest will be a molten, hydrostatic spheroid exposed to space. Initially, a quench crust will form very rapidly—a millimeter thick crust can form in ~minutes— but crustal growth slows down substantially once conduction replaces radiation as the rate-limiting step. Preventing fresh crust from immediately sinking until a self-supporting crust can form is beyond the scope of this paper, but as discussed in Section 1, the meteorite record suggests that this took place on some metallic bodies. Moreover, crystallization from the top down, rather than from the bottom up, is expected based on the expected liquidus and adiabat slopes (Williams, 2009). Once a strong crust forms, in the absence of core superheat and volcanism its thickness h will grow according to the Stefan solution (Turcotte & Schubert, 2014), approximated by $h \approx 20 \text{ km}(t/1 \text{ Myr})^{1/2}$. For these very approximate values, the time to form a 20 km crust is roughly one Myr.

This evolution can be more complicated if the simple top-down conductive cooling of the Stefan problem does not apply (Scheinberg et al., 2016). Advection is one way to modify this picture, but as discussed later fluid eruption is not expected to significantly alter the thermal behavior. Delamination at the base of the crust can also modify the thermal evolution of the body by maintaining a thinner crust. However, although delamination is likely to occur, Neufeld et al. (2019) show that neither it nor core superheat significantly modify the overall thermal evolution of the body, and that the Stefan assumption is generally justified.

3 Volcanic Cycle

Having discussed thermal evolution, we now move on to a discussion of how metallic volcanism might arise. The eruption process we describe takes place in three major stages, depicted in cartoon form in Figure 1. As the crust solidifies, the decrease in volume associated with the phase change results in radial contraction and compression. The second stage occurs when this stress exceeds the friction on existing faults, those faults move, and local low-stress regions surrounding the faults arise. The interior melt is then able to force open these cracks and migrate through them. The third stage describes when the liquid interior, which now has a decreased volume, causes sufficient contraction to close the cracks again and re-establish local compression.

3.1 Stage 1: Stress evolution due to bulk solidification

New solid will occupy a smaller volume than the melt from which it formed, and the resulting radial contraction generates compression. The deeper, hotter solid (the deeper ~half of the crust) will be ductile and able to viscously relax away this stress, while the colder upper layers will either deform elastically or undergo brittle failure. Because the crust will be in compression, volcanism will tend to be suppressed. To erupt, melt needs to force open cracks which are being held together by compressive stresses. It is important to note that

both Mercury and the Moon host volcanism despite globally compressive stress environments (Head & Wilson, 1992; Klimczak et al., 2018), so silicate volcanism can - at least locally and temporarily - overcome compression.

For a nominal 10 km crust with a linear thermal gradient, that gradient is $\frac{dT}{dz} \approx 10^{-1} \text{K/m}$.

This corresponds to a radial contraction (due to crystallization) of

$$h \frac{\Delta\rho}{\rho} = \frac{k \frac{dT}{dz} \Delta\rho}{L\rho} \approx 10^{-10} \text{m/s},$$

where L is latent heat and k is thermal conductivity. Note that part of the contraction is due to the entire crust cooling as the thermal profile gets longer, which has a similar magnitude to the contraction due to crystallizing so we fold it into our already very approximate ρ . This volume loss corresponds to a strain rate of

$$\dot{\epsilon} = h \frac{\Delta\rho}{\rho} / R \sim 10^{-15} \text{s}^{-1}.$$

This strain rate will evolve substantially with the crustal thickness; output from a simple numerical model of solidification-derived strain yields comparable results and is depicted in Figure 2.

3.2 Stage 2: Dike Formation

3.2.1 Dike Opening in Brittle Crust by Magma Ocean Overpressure—Light fluid underlying a dense crust will experience an upwards buoyancy pressure. This pressure is given by

$$P_{ex} = gh\Delta\rho \quad (1)$$

where h is the thickness of the crust and ρ is the density contrast between the crust and the liquid interior. This quantity is likely of order a few percent of ρ and is a combination of contraction due to crystallization, contraction due to cooling, and light element exclusion during crystallization. For an eruption to occur, this excess pressure must exceed compressional stresses in the elastic crust. Assuming the crust is already fractured, the stress to move a lithospheric fault (i.e. the maximum differential stress that can be present in the lithosphere) for the nominal crustal thickness of 10 km is given by Turcotte & Schubert (2014)

$$\sigma_{max} = \frac{2f_s \rho g h}{(1 + f_s^2)^{1/2} - f_s} \quad (2)$$

$$\approx \frac{\rho}{4} g h \approx 2 \text{ MPa} \quad (3)$$

where $f_s \approx 0.65$ is the coefficient of friction on crustal faults. This indicates that the lithosphere is able to support compressional stresses about $\frac{\rho/4}{\Delta\rho} \approx 10$ times larger than the excess hydrostatic pressure produced by its weight on the molten interior. However, contraction can easily exceed this stress and cause faults to fail. With E as Young's Modulus, the strain required is $\frac{\sigma_{max}}{E} \approx \frac{2 \times 10^6}{10^{11}} = 2 \times 10^{-5}$, which accumulates in $\frac{2 \times 10^{-5}}{10^{-15} \text{s}^{-1}} \approx 1 \text{ kyr}$, so

faults will frequently move and relieve stress. Assuming that fault motion is able to relieve most of the accumulated stress (Fulton et al., 2013) within a local area, the excess fluid pressure can then force cracks open during such periods.

3.2.2 Fracture Initiation in Ductile Crust—We argued above that melt ascent through the brittle section of the crust is possible, locally and temporarily, despite the overall compressional stress environment. However, the melt needs to be able to first ascend into the brittle region of the crust, which requires propagation through the nominally ductile lower crust. If partial melt is present in this region, porous flow may feed shallower, macroscopic dikes (Rubin, 1998). Below we will discuss the initiation of fractures at (or near) the base of the crust in the absence of partial melt, and then their ability to propagate under the influence of inflowing melt.

One problem that has to be overcome to form a fracture is the ductility of the iron near the base of the crust. Near its melting point, solid iron has a viscosity of $\sim 10^{11} \text{Pa} \cdot \text{s}$ (Frost & Ashby, 1982) and thus a viscoelastic response (Maxwell) timescale of 1 s, so for it to respond in a brittle fashion, the strain rate has to exceed 1 s^{-1} . The other major difficulty is the fact that iron has a high tensile strength, on the order of 100 MPa (Ashby, 1999, Figure 4.4), so large stresses are needed for fractures to form. These factors make fracture propagation much more challenging than the equivalent problem in silicate settings (Jellinek & DePaolo, 2003; Karlstrom & Richards, 2011, e.g.).

The most likely way to generate large stresses quickly is from cratering. Peak pressures on the order of hundreds of MPa occur to depths of 10 to 100 times the impactor radius, depending on the impact velocity (Melosh, 1989, Section 5.2). Thus, for impactors with radii around 1 km, fractures should extend through to the base of the crust while it is still only tens of kilometers thick. The role of impacts in volcanism is observed elsewhere in the solar system, particularly on Mercury where volcano occurrence is strongly associated with craters (Klimczak et al., 2018).

3.2.3 Dike Propagation—Once a fracture has formed, it will propagate if the forces trying to extend it exceed the forces resisting that extension. The fluid in the fracture is buoyant, generating stresses which tend to elongate the dike. The stress from buoyancy grows with dike length, so this force becomes more important in longer dikes. Strength in the host material serves to limit growth, because fracturing at the tip of the dike is required for its extension (Rubin, 1995). A compressional background stress increases the buoyancy required for a dike to propagate. Crawford & Stevenson (1988) derive an expression for the minimum length a dike must reach before pressure from melt buoyancy can fracture the crust and force the crack to open further. A dike will propagate itself when

$$K_c = (\pi I_{crit})^{1/2} [T + 2g\Delta\rho l_{crit}/\pi] \quad (4)$$

Here T is the local stress in the crust, defined here to be positive for tensile stress, K_c is the fracture toughness, and I_{crit} is the minimum length for a dike to become self propagating. To propagate itself vertically against 100 kPa of compressive stress ($\sim 5\%$ of what faults can support), a dike would have to be 11 km long. If, on the other hand, there were 200 kPa of

extensional stress, this critical length is less than 1 km. At $T=0$ the expression reduces to the result from Lister & Kerr (1991),

$$l_{crit} = \left(\frac{K_c}{\Delta\rho g} \right)^{2/3} \approx 7 \text{ km} \quad (5)$$

Even modest compressional stresses therefore result in critical crack lengths larger than the thickness of the entire crust. We thus conclude that the only time dike propagation is likely to occur is immediately after a faulting event has reduced the local compressional stress to approximately zero.

Dikes will be much more easily able to propagate if there is local tensile stress. There are at least two ways to generate local tensile stress which we expect to be present. One is impact craters. However, although we do not rule these out entirely, craters which are sufficiently large to generate rebound and tensile stresses near the base of the crust are likely to be uncommon. An alternative is for material to delaminate (i.e. detach and descend as a diapir) from the base of the crust, imparting rapidly-changing stresses to the material immediately above. Solid material tends to delaminate from the crust because it is more dense than the melt immediately below it, and at the base of the crust temperatures are high enough, and thus viscosities low enough, for material to flow. Delamination has been discussed on Io (Kirchoff & McKinnon, 2009), as well as on metallic asteroids (Neufeld et al., 2019), and in the latter case is expected to recur on timescales of a few tens of kyr. The stress will vary in and around the diapir, but Kirchoff & McKinnon (2009) point out that its magnitude is roughly $\sigma \sim \rho g \lambda$ where λ is the thickness of the layer being shed.

Based on Neufeld et al. (2019), the diapirs will have a length scale of about 1 km. Thus, delamination will generate stresses of order 100 kPa. Delamination also has the advantage of being a recurrent phenomenon, so the base of the crust is constantly being stressed and unstressed.

Assuming fluid injection timescales of tens of kyr, the bottom 60% of the crust is expected to be dominated by viscous processes, potentially leading to the growth of larger intrusions than the initial dikes (cf. Karlstrom et al., 2017). Such intrusions, however, would still be buoyant relative to the solid crust, and thus likely to ascend promptly (e.g. as diapirs), rather than being stored.

3.2.4 Dike Refreezing During Ascent—Melt forced upward through a crack will lose heat to crack walls and eventually refreeze. For eruptions to occur, the timescale of freezing needs to be longer than the timescale of melt ascent (e.g. Petford et al., 1994). Given the low viscosity of iron, the flow may be turbulent, in which case for a dike of width D the ascent velocity is given by (Wilson & Head, 2017):

$$u = \sqrt{D \frac{g}{f_d} \frac{\Delta\rho}{\rho}} \quad (6)$$

where f_d is the coefficient of drag on the crack walls. To refreeze, we need the dike walls to absorb a heat per area of $D\rho L$, where L is the latent heat of freezing. For eruption timescale t

and thermal diffusivity κ , this will propagate a distance $\sqrt{\kappa t} = \sqrt{\kappa h/u}$ into the walls, carrying away a heat per area of $C_p \rho \Delta T \sqrt{\kappa t}$, where C_p is the heat capacity of the walls. Setting these equal gives the width of the smallest crack that will refreeze

$$D_{min} = \left(\left(\frac{C_p \Delta T}{L} \right)^4 \frac{(kh)^2}{g} \frac{f_d}{\sim 1 \text{ m}^5 \sim 10^{-1}} \frac{\rho}{\sim 10^{1.5}} \right)^{1/5} \approx 0.3 \text{ m} \quad (7)$$

where here we have taken $h=10$ km, $g=0.1$ m s⁻². This minimum width is similar to Earth, where basalt has a minimum width of 1 meter (Rubin, 1995), so reasonable width cracks are able to avoid refreezing. Assuming a viscosity of 10^{-2} Pa · s, these values give us a Reynolds number greater than 10^3 , so using the turbulent velocity is appropriate.

3.3 Stage 3: Dike Closing, Reestablishing Compressional Regime

3.3.1 Eruption Volume—Eruptions are self-limiting processes, because compressional stress reaccumulates as the liquid volume reduces and the crust subsides. An eruption will stop when the stress in the crust is equal to the excess pressure in the ocean ($gh - \rho$). If, at the beginning of an eruption, the difference between the ocean excess pressure and the local crustal stress is P_{net} , then assuming the interior melt only compresses elastically (i.e. has zero volatile content), a corresponding strain of $\epsilon = \frac{P_{net}}{E}$ will accumulate. Treating the eruption as a layer covering the entire body with thickness δ , then $\epsilon \approx \frac{\delta}{R}$. If we assume that faulting has relieved all compressional stress in the crust, $P_{net} = gh - \rho$ and

$$\delta = \frac{gh \Delta \rho R}{E} = \frac{4}{3} \pi G h \rho \Delta \rho R^2 \quad (8)$$

$$= 0.3 \text{ m} \times \left(\frac{\Delta \rho}{150 \text{ kg/m}^3} \right) \left(\frac{R}{100 \text{ km}} \right)^2 \left(\frac{h}{10 \text{ km}} \right) \left(\frac{10^{11} \text{ Pa}}{E} \right) \quad (9)$$

If some stress remains in the crust this value will be diminished somewhat. The nominal value of δ implies an eruption volume V_{erupt} of 40 km^3 .

Eruptions will advect heat equal to $V_{erupt} \rho (C_p \Delta T + L) \approx 10^{20} \text{ J}$. With a surface thermal gradient of 0.1 K/m this is roughly 10 years of global conductive heat loss. The importance of advection thus depends on how frequently those eruptions occur relative to this 10 year value.

3.3.2 Eruption Interval—After an eruption, compressional crustal stress will be reestablished and the crust will once again need to accumulate $\sigma \approx \frac{\rho g h}{4} \approx \rho^2 h G R$ stress (as discussed in stage 2, above) before this particular fault will fail again. New solid plated onto the base of the crust with thickness h , will create a strain

$$\epsilon = \frac{\Delta h \Delta \rho}{R \rho} \quad (10)$$

which can be rearranged to solve for the thickening required to cause the next failure

$$\Delta h = \frac{\frac{\pi}{3} \rho^3 R^2 h G}{\Delta \rho E} \approx 150 \text{ m} \times \left(\frac{150 \text{ kg/m}^3}{\Delta \rho} \right) \left(\frac{R}{100 \text{ km}} \right)^2 \left(\frac{h}{10 \text{ km}} \right) \left(\frac{10^{11} \text{ Pa}}{E} \right) \quad (11)$$

Using $\Delta t \approx \frac{2h\Delta h}{\kappa}$ we end up with failure every few kyr. The fact that this is large compared to the 10 years above means that eruptions do not play a significant role in the thermal evolution of the body.

This process differs from volcanic stress accumulation on Earth. On Earth, magma chamber stresses can transition from elastic/brittle- to viscously-accommodated as the thermal environment around the magma chamber changes (Jellinek & DePaolo, 2003). In our case, stress arises from global volume changes associated with solidification, and the thermal environment across the crust changes only very slowly: viscous relaxation is always rapid at the base of the crust (Sec 3.2.2), and always negligible at the surface.

Note that in both of the previous sections we treated these processes as if all of the planet's stress accumulation and relief occurs on a single fault, which is certainly not the case. In reality, faulting and erupting depends fundamentally on local stress evolution, so global stress does not directly capture these events. The value of treating eruptions this way is that it captures the relative volumes of erupted and deeply crystallized material, and thus reflects the role of eruptions in the body's overall thermal evolution.

3.3.3 Total Erupted Volume—A useful value to look at is the erupted layer thickness, δ , divided by the thickness of plating needed for eruption, h ,

$$\frac{\delta}{\Delta h} = \frac{\frac{4}{3} \pi G h \rho \Delta \rho R^2 / E}{\frac{\pi}{3} \rho^3 R^2 h G / \Delta \rho E} \quad (12)$$

$$= \left(2 \frac{\Delta \rho}{\rho} \right)^2 \approx 10^{-3} \quad (13)$$

Importantly, most of the uncertain parameters that went into δ and h cancel (note that the E in the numerator and the denominator only cancel if the liquid and solid have similar elastic moduli, which may not be the case in the presence of volatiles, as discussed below). This means that although erupted volumes and frequencies are very uncertain, the total amount of material that can be erupted is much better constrained. This value is an upper limit, because it reflects the volume fraction of the body to participate in eruptions if every faulting event relieves all local compressional stress and leads to an eruption. The real value is likely to be smaller. One thousandth of the body as an upper limit on material erupted means that eruptions will not play a major role in thermal and stress evolution, serving only to modify

the surface. This is in contrast to, for example, Io, where volcanism is the dominant source of heat transfer (e.g. Moore, 2001).

4 Role of Volatiles

There are two important ways that volatiles can alter the behavior of iron volcanism. The first is the fact that they will be excluded from the crystallizing solid, making the melt more buoyant than implied by just the phase transition and thermal contraction. Sulfur in particular is likely to be present (Chabot & Haack, 2006) and can be expected to play this role, but its concentration is a major unknown. In an extreme case, native sulfur might erupt, in a similar manner to the sulfur volcanism proposed for Io (Sagan, 1979; Williams et al., 2001), but eruption of an Fe-S alloy is much more likely. Any light elements present in the melt should serve to enhance volcanism.

The second way that volatiles can be important parallels a role they play in silicate magmatism, and likely play in cryovolcanism. As pressure is relieved during eruptions, volatiles may exsolve and form bubbles, lowering the density of the melt column, accelerating its ascent and also increasing its compressibility (Bower & Woods, 1997). This process is difficult to predict because it not only requires knowing the initial volatile content of the iron, but also the tendency of those volatiles to exsolve. Further complicating this is the fact that mantle stripping is a violent process (Asphaug et al., 2006) which may have already exposed the bulk of the core to vacuum, removing volatiles which could provide a bubble source. We therefore do not pursue this issue any further here.

5 Geomorphic Implications and Potential Constraints from Observation

Identifying iron volcanoes on metallic asteroids may prove to be challenging. Searches for cryovolcanism motivate caution in interpreting features as volcanic in origin: Moore & Pappalardo (2011) provide a summary of several past mistaken identifications of cryovolcanism, an important warning for further searches for volcanoes. In addition, any such volcanoes have had more than 4 billion years to be modified. 16 Psyche, for example, is far from hydrostatic (Shepherd et al., 2017), and if not a rubble pile must at least be heavily altered by impacts.

In the event that metallic volcanoes can be identified using present-day observations, they will likely be very informative. For example, it is likely that volcanoes will be spatially associated with impact craters, analogous to what is seen on Mercury (Klimczak et al., 2018), and the degree of this association will inform the stress evolution of the crust. A rapidly-cooling metallic flow may acquire a remanent magnetic field, if an internal dynamo is active at that time (Bryson et al., 2015). Similarly, the style of volcanism on the body alone provides substantial insight. Because there is no analog to the buoyant continental crust on Earth, the development of large mid-crustal magma chambers and calderas is less likely on iron asteroids, so sill and lacolith formation are unlikely to occur. However, if there is silicate material or a porous mega-regolith overlying the bulk metallic crust, intrusive volcanism at the metal-silicate interface, perhaps leading to diapirism, may occur. This situation is briefly addressed in Johnson et al. (2019) and warrants further work. If the

volcanism is effusive, we expect it to form thin, laterally-extensive deposits as a result of liquid iron's low viscosity (Griffiths, 2000). If the volcanism is explosive, the eruptive behavior will depend on the volatiles present and the reservoir conditions (Bower & Woods, 1997; Lu & Kieffer, 2009) and will have major implications for light element incorporation in cores, volatile retention during mantle stripping, and devolatilization during subsequent evolution. We caution, however, that in the latter case the eruption velocity could easily exceed the escape velocity (≈ 200 m/s) making identification of volcanic deposits more challenging than on e.g. Mercury.

6 Evidence in the Meteorite Record

A key prediction that follows from metallic volcanism is that bodies hosting it will have two end-member types of solids which experienced very different histories. Material crystallizing onto the bottom of the crust will cool slowly and will exhibit an inverse correlation between cooling rate and light element content. Erupted material will crystallize very quickly, and unless it is reheated will show \sim instantaneous cooling. This quenching will prevent elemental fractionation, so erupted material will record the (non-volatile) element abundances of the liquid interior at the time it was erupted. Incompatible element (Ga, Ge, Ir, etc.) concentrations will be much larger than contemporaneously formed deep solids. These meteorites would likely be some of the most incompatible element enriched material in their meteorite family. If volatile exsolution is involved, the quenched solids would likely contain vesicles. However, because erupted material is a small volume fraction of the body, the quenched meteorites will likely be rare. Although a detailed analysis is beyond the scope of this paper, it is plausible that the modern meteorite record can serve as a test of this paper's predictions.

It is important to note that there are important differences between how silicate and iron cooling and crystallization are recorded in hand specimens. Most of the visible texture in iron meteorites is the result of sub-solidus processes (Hutchison, 2004; Wasson, 1985), which can be used to determine cooling rates (Sec 1). Chemical and/or textural evidence of crystallization itself (e.g. dendrites) may be retained, but is predicted to vary on length-scales much larger than almost all available iron meteorite specimens (Haack & Scott, 2009), so no spatial information on crystallization is available.

7 Conclusions

We predict that some metallic asteroids will have hosted volcanic activity while solidifying. Overall, metallic volcanism should bear more resemblance to silicate volcanism than cryovolcanism. This is because, like silicates, the melt is buoyant, and the thermal conditions under which melt travels through dikes are similar. However, fracture initiation is more difficult in metallic systems because of the ductility and tensile strength of iron, while fracture growth is opposed by the large fracture toughness of iron and the background compressional environment. Apart from volatiles, the largest uncertainty in our analysis probably relates to dike initiation and propagation. This depends on the somewhat uncertain fracture toughness of the crust (Ashby, 1999), and the frequency of large enough stresses to cause fracturing and fracture propagation. At a minimum, large impacts should be able to

cause the crust to occasionally fail, but if delamination occurs, it is more likely to drive dike propagation and ferrovulcanism.

The details of the hypothesized processes will require substantial further theoretical investigation. Geomorphological examples of iron volcanoes would make for particularly striking confirmation, but will likely be very difficult, if not impossible, to unambiguously identify. More likely, testing of this hypothesis will come from the meteorite record, either by explaining existing anomalies in the record or predicting the characteristics of future meteorites.

Acknowledgments

Partial support from NASA-80NSSC18K0601 is acknowledged. The MS was originally submitted on 28 Nov 2018. We thank the reviewers, Dave Williams and Mark Jellinek, for their perceptive comments, and Denton Ebel for helpful advice on meteorite textures. This is a theoretical paper and no data were generated.

References

- Ahrens TJ, & Johnson ML. (1995). Shock wave data for minerals. *Mineral Physics & Crystallography: A Handbook of Physical Constants*, 2, 143–184.
- Albarède F, Bouchet RA, & Blichert-Toft J. (2013). Siderophile elements in IVA irons and the compaction of their parent asteroidal core. *Earth and Planetary Science Letters*, 362, 122–129. 10.1016/j.epsl.2012.11.059
- Ashby MF. (1999). *Materials selection in mechanical design*, Butterworth-Heinemann, Oxford, England.
- Asphaug E, Agnor CB, & Williams Q. (2006) Hit and run planetary collisions. *Nature*, 438, 155–160. 10.1038/nature04311
- Bottke WF, Durda DD, Nesvorný D, Jedicke R, Morbidelli A, Vokrouhlický D, Levison HF. (2005). Linking the collisional history of the main asteroid belt to its dynamical excitation and depletion. *Icarus*, 179, 63–94. 10.1016/j.icarus.2005.05.017
- Bower SM & Woods AW. (1997). Control of magma volatile content on the mass erupted during explosive volcanic eruptions Saturated magma. *Journal of Geophysical Research*, 102, 10273–10290. 10.1029/96JB03176
- Bryson JFJ, Nichols CIO, Herrero-Albillos J, Kronast F, Kasama T, Alimadadi H, ... Harrison RJ. (2015). Long-lived magnetism from solidification-driven convection on the pallasite parent body. *Nature*, 517(7535), 472–475. 10.1038/nature14114 [PubMed: 25612050]
- Carlslaw HS, & Jaeger JC. (1959). *Conduction of heat in solids*. Oxford Science Publications (p. 497). Oxford, England.
- Chabot NL, & Haack H. (2006). *Evolution of Asteroidal Cores Meteorites and the Early Solar System II*, University of Arizona Press, 747–771.
- Crawford GD, & Stevenson DJ. (1988). Gas-driven water volcanism and the resurfacing of Europa. *Icarus*, 73(1), 66–79. 10.1016/0019-1035(88)90085-1
- Frost HJ, & Ashby MF. (1982). *Deformation-mechanism maps: The plasticity and creep of metals and ceramics*, Pergamon Press, Oxford, England.
- Fulton PM, Brodsky EE, Kano Y, Mori J, Chester F, Ishikawa T, et al. (2013). Low coseismic friction on the Tohoku-Oki fault determined from temperature measurements. *Science*, 342(6163), 1214–1217. 10.1126/science.1243641 [PubMed: 24311684]
- Goldstein JI, Scott ERD, & Chabot NL. (2009). Iron meteorites: Crystallization, thermal history, parent bodies, and origin. *Chemie Der Erde*, 69(4), 293–325. 10.1016/j.chemer.2009.01.002
- Griffiths RW. (2000). The dynamics of lava flows. *Annual Review of Fluid Mechanics*, 32, 477–518. 10.1146/annurev.fluid.32.1.477

- Haack H, Rasmussen KL, & Warren PH. (1990). Effects of regolith/megaregolith insulation on the cooling histories of differentiated asteroids, *J. Geophys. Res.*, 95(B4), 5111–5124, doi: 10.1029/JB095iB04p05111
- Haack H, Scott ERD. (2009). Asteroid core crystallization by inward dendritic growth. *Journal of Geophysical Research*, 97(E9), 14727–14734. 10.1029/92je01497
- Head JW, & Wilson L. (1992). Lunar mare volcanism: Stratigraphy, eruption conditions, and the evolution of secondary crusts. *Geochimica et Cosmochimica Acta*, 56(6), 2155–2175. 10.1016/0016-7037(92)90183-J
- Hevey PJ, & Sanders IS. (2006). A model for planetesimal meltdown by ²⁶Al and its implications for meteorite parent bodies. *Meteoritics & Planetary Science*, 41(1), 95–106. 10.1111/j.1945-5100.2006.tb00195.
- Hutchison R. (2004). *Meteorites: A petrologic, chemical and isotopic synthesis*. Cambridge Univ. Press, Cambridge, England.
- Jellinek AM, & DePaolo DJ. (2003). A model for the origin of large silicic magma chambers: Precursors of caldera-forming eruptions. *Bulletin of Volcanology*, 65(5), 363–381. 10.1007/s00445-003-0277-y
- Jellinek AM, & Kerr RC. (2001). Magma dynamics, crystallization, and chemical differentiation of the 1959 Kilauea Iki lava lake, Hawaii, revisited. *Journal of Volcanology and Geothermal Research*, 110(3–4), 235–263. 10.1016/S0377-0273(01)00212-8
- Johnson BC, Sori MM, & Evans AJ. (2019). Ferrovolcanism, Pallasites, and Psyche. *Lunar and Planetary Science Conference L*, abstract #1625.
- Karlstrom L, Paterson SR, & Jellinek AM. (2017). A reverse energy cascade for crustal magma transport. *Nature Geoscience*, 10(8), 604–608. 10.1038/NGEO2982
- Karlstrom L, & Richards M. (2011). On the evolution of large ultramafic magma chambers and timescales for flood basalt eruptions. *Journal of Geophysical Research: Solid Earth*, 116(8), 1–13. 10.1029/2010JB008159
- Kirchoff MR, & McKinnon WB. (2009). Formation of mountains on Io: Variable volcanism and thermal stresses. *Icarus*, 201(2), 598–614. 10.1016/j.icarus.2009.02.006
- Klimczak C, Crane KT, Habermann MA, & Byrne PK. (2018). The spatial distribution of Mercury's pyroclastic activity and the relation to lithospheric weaknesses. *Icarus*, 315, 115–123. 10.1016/j.icarus.2018.06.020
- Lister JR, & Kerr RC. (1991). Fluid-mechanical models of crack propagation and their application to magma transport in dykes. *Journal of Geophysical Research*, 96(B6), 10049–10077. 10.1029/91JB00600
- Lopes RMC & Gregg TKP (2004). *Volcanic worlds: Exploring the solar system's volcanoes*, Springer, 235.
- Lord P, Tilley S, Oh DY, Goebel D, Polansky C, Snyder S, ... Elkins-Tanton L. (2017). Psyche: Journey to a metal world. *IEEE Aerospace Conference Proceedings*, 2014, 1–11. 10.1109/AERO.2017.7943771
- Lu X, & Kieffer SW. (2009). Thermodynamics and mass transport in multicomponent, multiphase H₂O Systems of Planetary Interest. *Annual Review of Earth and Planetary Sciences*, 37(1), 449–477. 10.1146/annurev.earth.031208.100109
- Manga M, & Wang CY. (2007). Pressurized oceans and the eruption of liquid water on Europa and Enceladus. *Geophysical Research Letters*, 34(7), 1–5. 10.1029/2007GL029297
- Matter A, Delbo M, Carry B, & Ligorì S. (2013). Evidence of a metal-rich surface for the Asteroid (16) Psyche from interferometric observations in the thermal infrared. *Icarus*, 226(1), 419–427. 10.1016/j.icarus.2013.06.004
- Melosh HJ. (1989). *Impact cratering, a geologic process* Oxford Univ. Press, New York, United States.
- Moore WB. (2001). The thermal state of Io. *Icarus* 154, 548–550. 10.1006/icar.2001.6739
- Moore JM, & Pappalardo RT. (2011). Titan: An exogenic world? *Icarus*, 212(2), 790–806. 10.1016/j.icarus.2011.01.019
- Moore JM, McKinnon WB, Spencer JR. et al. (2016). The geology of Pluto and Charon through the eyes of New Horizons, *Science* 351, 1284–1293. 10.1126/science.aad7055 [PubMed: 26989245]

- Neeley JR, Clark BE, Ockert-Bell ME, Shepard MK, Conklin J, Cloutis EA, ... & Bus SJ. (2014). The composition of M-type asteroids II: Synthesis of spectroscopic and radar observations. *Icarus*, 238, 37–50. 10.1016/j.icarus.2014.05.008
- Neufeld JA, Bryson JFJ, & Nimmo F. (2019). The top-down solidification of iron asteroids driving dynamo evolution. *Journal of Geophysical Research: Planets*. In review.
- Nimmo F, & Spencer JR. (2015). Powering Triton's recent geological activity by obliquity tides: Implications for Pluto geology, *Icarus* 246, 2–10. 10.1016/j.icarus.2014.01.044
- Petford N, Kerr RC, & Lister JR. (1993). Dike transport of granitoid magmas. *Geology*, 21(9), 845–848. 10.1130/0091-7613(1993)021<0845:DTOGM>2.3.CO;2
- Porco ACC, Helfenstein P, Thomas PC, Ingersoll AP, Wisdom J, West R, ... Johnson VT. (2006). Cassini observes the active south pole of Enceladus, 311, 1393–1401. 10.1126/science.1123013
- Roth L, Saur J, Retherford KD, Strobel DF, Feldman PD, McGrath MA, & Nimmo F. (2014). Transient water vapor at Europa's south pole. *Science*, 343(6167), 171–174. 10.1126/science.1247051 [PubMed: 24336567]
- Rubin AM. (1995). Propagation of Magma-Filled Cracks. *Annual Reviews*, 215–217. 10.1146/annurev.ea.23.050195.001443
- Rubin AM. (1998). Dike ascent in partially molten rock. *Journal of Geophysical Research: Solid Earth*, 103, 20901–20919. 10.1029/98JB01349
- Sagan C. (1979). Sulphur flows on Io. *Nature*, 280, 750–753. 10.1038/280750a0
- Scheinberg A, Elkins-Tanton LT, Schubert G, & Bercovici D. (2016). Core solidification and dynamo evolution in a mantle-stripped planetesimal. *Journal of Geophysical Research: Planets*, 121(1), 2–20. 10.1002/2015JE004843
- Schenk PM, McKinnon WB, Gwynn D, Moore JM. (2001) Flooding of Ganymede's bright terrains by low-viscosity water-ice lavas, *Nature* 410, 56–60. 10.1038/35065027
- Shepherd MK, Richardson J, Taylor PA, Rodrigues-Ford LA, Conrad A. de Pater I, et al. (2017). Radar observations and shape model of asteroid 16 Psyche. *Icarus*, 281, 388–403. 10.1016/j.icarus.2016.08.011
- Tkalcec BJ, Golabek GJ, Brenker F, (2013). Solid-state plastic deformation in the dynamic interior of a differentiated asteroid, *Nature Geoscience*. 6, 93–97. 10.1038/ngeo1710
- Turcotte DL, & Schubert G. (2014), *Geodynamics*, Cambridge Univ. Press, Cambridge, England.
- Wasson JT, *Meteorites: Their Record of Early Solar-System History*, 267, W.H. Freeman Press, New York, 1985.
- Williams DA, Greeley R, Lopes RMC, & Davies AG. (2001). Evaluation of sulfur flow emplacement on Io from Galileo data and numerical modeling. *Journal of Geophysical Research E: Planets*, 106(E12), 33161–33174. 10.1029/2000JE001340
- Williams Q. (2009). Bottom-up versus top-down solidification of the cores of small solar system bodies: Constraints on paradoxical cores. *Earth and Planetary Science Letters*, 284(3–4), 564–569. 10.1016/j.epsl.2009.05.019
- Wilson L. (2009). Volcanism in the solar system, *Nature Geosci.* 2, 389–397. 10.1038/ngeo529
- Wilson L, & Head JW. (2017). Generation, ascent and eruption of magma on the Moon: New insights into source depths, magma supply, intrusions and effusive/explosive eruptions (Part 1: Theory), *Icarus* 283, 146–175. 10.1016/j.icarus.2015.12.039
- Yang J, Goldstein JI, & Scott ERD. (2008). Metallographic cooling rates and origin of IVA iron meteorites. *Geochimica et Cosmochimica Acta*, 72, 3043–3061. 10.1016/j.gca.2008.04.009
- Yang J, & Goldstein JI. (2006). Metallographic cooling rates of the IIIAB iron meteorites. *Geochimica et Cosmochimica Acta*, 70(12), 3197–3215. 10.1016/j.gca.2006.04.007
- Yang J, Goldstein JI, & Scott ERD. (2007). Iron meteorite evidence for early formation and catastrophic disruption of protoplanets. *Nature*, 446, 888–891. 10.1038/nature05735 [PubMed: 17443181]

Key Points:

- Metallic asteroids begin fully molten, and as they solidify their remaining melt is buoyant.
- The primary stress state of metallic asteroid crust is compression, limiting the ability of melt at depth to reach the surface.
- Local stress changes likely allow this compression to be overcome, and we predict metallic asteroids should host volcanic activity.

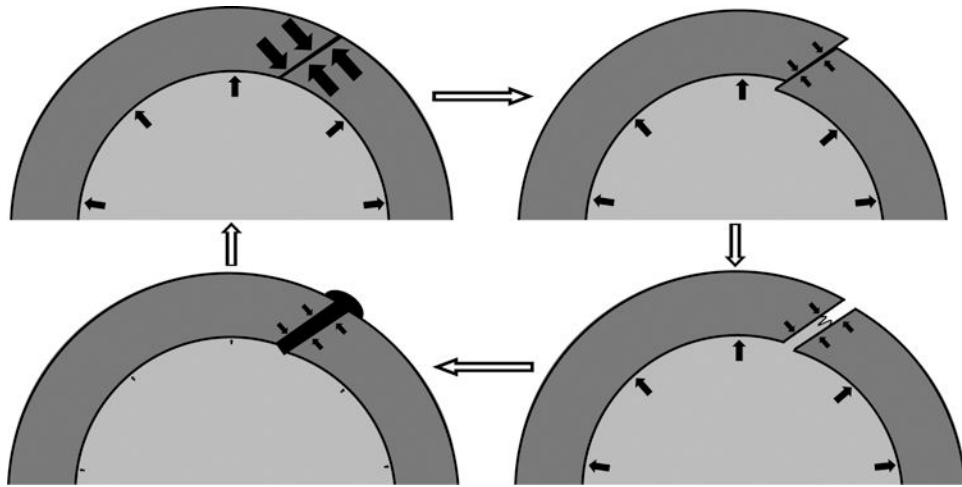


Figure 1.

Cartoon depicting the volcanic cycle we describe. Beginning in the top-left is the typical state of the crust, where compressional stress prevents the melt at depth from reaching the surface. Volcanism then begins with a faulting event and the resulting decreased local compressional stress in the crust is no longer larger than hydrostatic pressure. Next, the liquid interior forces open the fault and melt migrates through the newly formed dike. Finally, melt reaches the surface and the now-depressurized ocean is no longer able to support the crust, causing the crack to close again. Subsequent crustal growth increases contraction in the crust slowly until faulting can occur again.

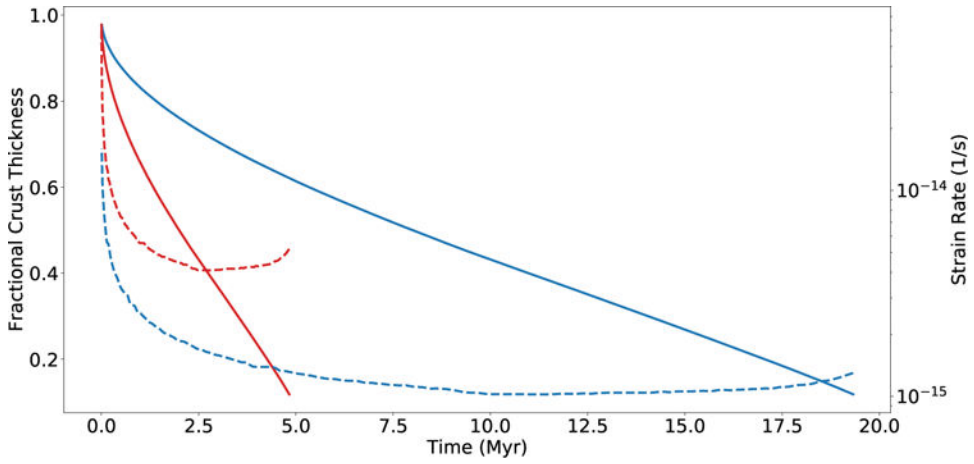


Figure 2.

Evolution of an initially molten spherical iron body. Solid lines show the thickness of solid crust as a fraction of body radius and dashed lines show smoothed strain rate due to surface contraction. Red lines are for a 100 km radius body and blue lines are for a 200 km radius body. This model uses the approach of Nimmo & Spencer (2015) to numerically solve the Stefan problem with the surface pinned to 200 K, the liquid interior at 1200 K and other parameter values given in Table 1. Models taking core superheat and delamination into account (Neufeld et al., 2019) yield similar results

Table 1.

Parameters Used

	Description	Value	Source
κ_s	Silicate thermal diffusivity	$1.1 \times 10^{-6} \text{ m}^2/\text{s}$	(Carslaw & Jaeger, 1959)
κ_m	Metal thermal diffusivity	$1.2 \times 10^{-5} \text{ m}^2/\text{s}$	(Carslaw & Jaeger, 1959)
T_m	Melting point	1200 K	Assumed
T_s	Temperature due to solar irradiation	200 K	Assumed
L	Latent heat	$2.7 \times 10^5 \text{ J/kg}$	(Haack et al., 1990)
C_p	Specific heat capacity	569 J/kg·K	(Carslaw & Jaeger, 1959)
Q	Activity energy	$2.5 \times 10^5 \text{ J/mol}$	(Frost & Ashby, 1982)
R_g	Gas constant	8.314 J/mol·K	
R	Body Radius	100 km	Assumed
g	Acceleration due to gravity	[m/s ²]	
ρ	Density	7400 km/m ³	(Carslaw & Jaeger, 1959)
ρ	Density contrast between melt and solid	$\approx \rho/40$	Assumed, very approximate
h	Crust thickness	[m]	
h_e	Elastic/brittle crustal layer thickness	$h/2$	Calculated, approximate
P	Pressure	[Pa]	
f_s	Coefficient of friction on faults	0.65	(Turcotte & Schubert, 2014)
f	Drag coefficient in dikes	0.1	Assumed
σ	Stress	[Pa]	
ϵ	Strain	dimensionless	
$\dot{\epsilon}$	Strain Rate	[s ⁻¹]	
K	Bulk Modulus	10^{11} Pa	(Ahrens & Johnson, 1995)
K_c	Fracture Toughness	$10^7 \text{ Pa}\cdot\text{m}^{1/2}$	(Ashby, 1999, Figure 4.7)
D	Dike width	[m]	
h	Crystallized layer thickness	[m]	
δ	Erupted layer thickness if global	[m]	
l_{crit}	Dike Critical Length	[m]	(Crawford & Stevenson, 1988)
λ	Diapir Thickness	[m]	

Note that entries without values or without sources are outputs we are finding. Brackets indicate units when a specific value is not relevant.